

Phase-change materials: The view from the liquid phase and the metallicity parameter

Shuai Wei, Pierre Lucas, and C. Austen Angell

While fast-switching rewritable nonvolatile memory units based on phase-change materials (PCMs) are already in production at major technology companies such as Intel (16–64 GB chips are currently available), an in-depth understanding of the physical factors that determine their success is still lacking. Recently, we have argued for a liquid-phase metal-to-semiconductor transition (M-SC), located not far below the melting point, T_m , as essential. The M-SC is itself a consequence of atomic rearrangements that are involved in a fragile-to-strong viscosity transition that controls both the speed of crystallization and the stabilization of the semiconducting state. Here, we review past work and introduce a new parameter, the “metallicity” (inverse of the average Pauling electronegativity of a multicomponent alloy). When T_m -scaled temperatures of known M-SCs of Group IV, V, and VI alloys are plotted against their metallicities, the curvilinear plot leads directly to the composition zone of all known PCMs and the temperature interval below T_m , where the transition should occur. The metallicity concept could provide guidance for tailoring PCMs.

Introduction

Switching behavior of phase-change materials and the relevance of liquid states

For more than half a century, mixtures of elements in the non-metal section of the periodic table have been famous for their ability to form glasses (e.g., As-Se) from their liquid states, often with great stability, low acoustic losses, and high corrosion resistance. They have found many applications, particularly in infrared optics (e.g., night vision) and semiconductor electronics.¹ However, as the compositions tested include heavier elements (e.g., Se replaced by Te and As replaced by Sb), the glass-forming ability diminishes, seemingly as the bandgap decreases. While As_2Se_3 is extremely difficult to crystallize on laboratory time scales, Bi_2Te_3 is metallic and difficult to vitrify even by sputtering. In between the two is As_2Te_3 , which undergoes a semiconductor-to-metal transition when heated above its melting point, T_m .²

In 1968, Ovshinsky³ discovered that he could use the ability of Te-containing alloys to generate solid phases of greatly differing electronic conductivities depending on whether they were vitreous or crystalline, to make switching devices and memory devices. Apart from some excellent fundamental

studies in Ovshinsky’s laboratory, however, development was slow, with a resurgence of interest only in the late 1980s after Yamada et al.⁴ published a study on the three-component Ge-Sb-Te system that showed special behavior in fast phase switching and property contrasts along what we will call the “Yamada line,” (the composition line joining GeTe to Sb_2Te_3). The Yamada line,⁵ comprising the most popular phase-change materials (PCMs), features several closely related crystalline compounds with simple structures and remarkably fast crystallization kinetics. These crystalline compounds have been studied in detail by Wuttig, who in 2005, highlighted the storage potential of devices containing them.⁶ A follow-up 2007 paper on the subject by Wuttig and Yamada in collaboration,⁷ has been greatly cited. Recently, this interest has been translated into manufactured devices, and even more recently, attention has been directed to the liquid states of PCMs, in order to understand their special crystallization properties.^{8–12}

In this article, we review these liquid-state issues and then take the development one step further by introducing and exploiting a new material parameter, the “metallicity.” Using this parameter in our plots allows us to strengthen the claim that it is the existence of a metal-to-semiconductor transition

Shuai Wei, Institute of Physics, RWTH Aachen University, Germany; swei@physik.rwth-aachen.de
Pierre Lucas, Department of Materials Science and Engineering, The University of Arizona, USA; Pierre@u.arizona.edu
C. Austen Angell, School of Molecular Sciences, Arizona State University, USA; caa@asu.edu
doi:10.1557/mrs.2019.207

(M-SC) located at a critical distance below T_m that makes it possible for these PCMs to perform as they do.

First, we give a brief introduction to glass-forming liquid phenomenology. **Figure 1** illustrates both paradoxical and practical aspects of the typical glass-forming liquid, which is a liquid that is slow to crystallize on cooling below its T_m .^{7,13} Figure 1a shows how the excess entropy of the liquid introduced on melting decreases rapidly as supercooling is extended, as a consequence of the higher heat capacity of the liquid. It is evident that the entropy of the liquid would fall below that of the crystal far above 0 K were it not for the intercession of a structural arrest phenomenon, the “glass transition” (T_g), at which the heat capacity (C_p) contribution coming from configurational changes with temperature, drops out. The avoidance of a thermodynamic catastrophe by a kinetic phenomenon is known as the Kauzmann paradox; this has attracted much attention from the theory community.

On the other hand, in PCMs, which are poor glass formers, this scenario is only realized when the cooling rate is very high. The glassy state that is trapped would be high in entropy and low in stability relative to more slowly cooled structures if not assisted by some additional source of entropy loss. The additional source of entropy loss will be the focal point of this article.

The action of reheating the glass, by a heat pulse, to a temperature kept well below T_m provides a new opportunity for the glass to crystallize. The crystal, with more ordered structure and much higher electronic conductivity, can generate the “on” state of a microscopic “bit” of the material, which is illustrated by the red heat-and-cool arrow in Figure 1a. If the heat pulse is sufficient to raise the temperature above T_m , and the surrounding provides a good enough heatsink, then the cooling rate after the pulse will be sufficient to return the sample to the glassy, or “off,” state. In PCMs, this fine-tuned and complex sequence can be repeated countless times with high reproducibility, allowing for fabrication of a chip with huge memory storage capacity.^{14–16}

Figure 1b shows the relation of the liquidus surface of the Ge-Sb-Te system in relation to the composition of known PCMs,¹³ in particular, the Yamada line of crystals that has been given the most attention. The PCM compositions all have low T_m , but apparently not the lowest or PCMs would be concentrated at the ternary eutectic composition, which is the most easily glass forming.

No-man’s land of PCMs

The problem with identifying the additional source of entropy loss that was previously mentioned is that it clearly must occur below the T_m and, of course, well above T_g . The fact that the crystallization rates of PCMs, in contrast to the chalcogenide glass formers of earlier studies, are extremely high, means that it is difficult to characterize what the additional source of entropy loss might be by direct experiments. The problem is reminiscent of that of supercooled water, the “most anomalous liquid,” which has been the source of much interest because of the apparent existence of a transition of higher order, (close to first order), lying about 20% below the T_m .¹⁷

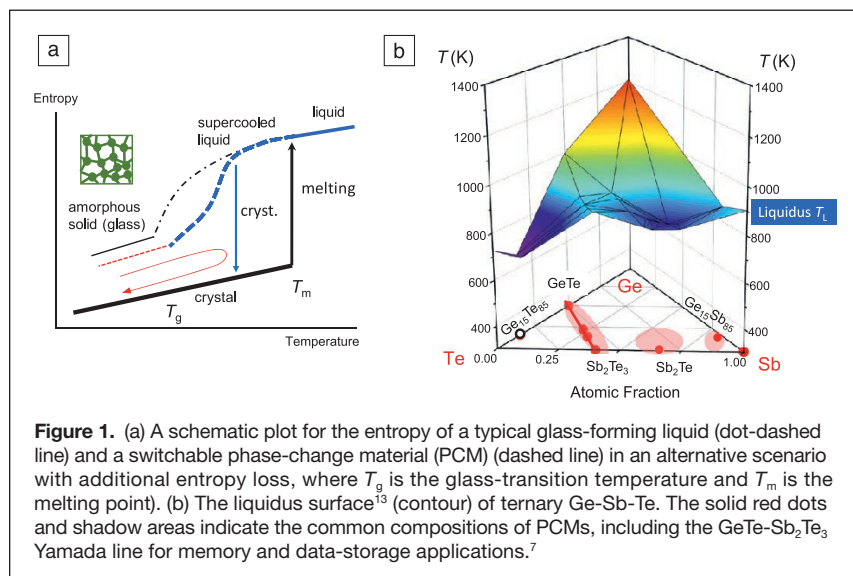
In the case of water, the thermodynamic properties, which are well known in the stable range between 0 and 100°C, develop striking anomalies as the liquid is supercooled. With samples of extreme cleanliness, these can be studied down to the “homogeneous nucleation temperature” T_h near -31°C for large (10 ml ampoules) and -38°C for micron-sized samples (special emulsions). The isothermal compressibility, for instance, increases according to a power law with an apparent divergence temperature of 228 K, implying proximity to a critical point.¹⁸ So far, comparable supercooling has not been reported for PCMs.

This undercooling limit on measurements near T_m , and corresponding termination of the glassy state due to fast crystallization at far lower temperatures, establishes the existence of a “no-man’s land” (a term used for the water problem) in which no observations can be made except by ultrafast

probes or deduction from external studies such as crystallization rates. In the next sections, we will make use of a simpler and more powerful approach using plausible extrapolations of the properties of many non-PCM, but related, materials, to reach the conclusions about the PCMs themselves. In this approach, we will be greatly aided by the metallicity parameter previously mentioned.

Thermodynamic response functions in Group IV, V, and VI liquid alloys Density and thermal expansivity anomalies

Three elements and many Group IV, V, and VI alloys exhibit temperatures of maximum density (T_{MD}) in their liquid states, an anomaly often mistakenly thought to be unique to water. In **Figure 2**,^{19–26} liquid densities are plotted against

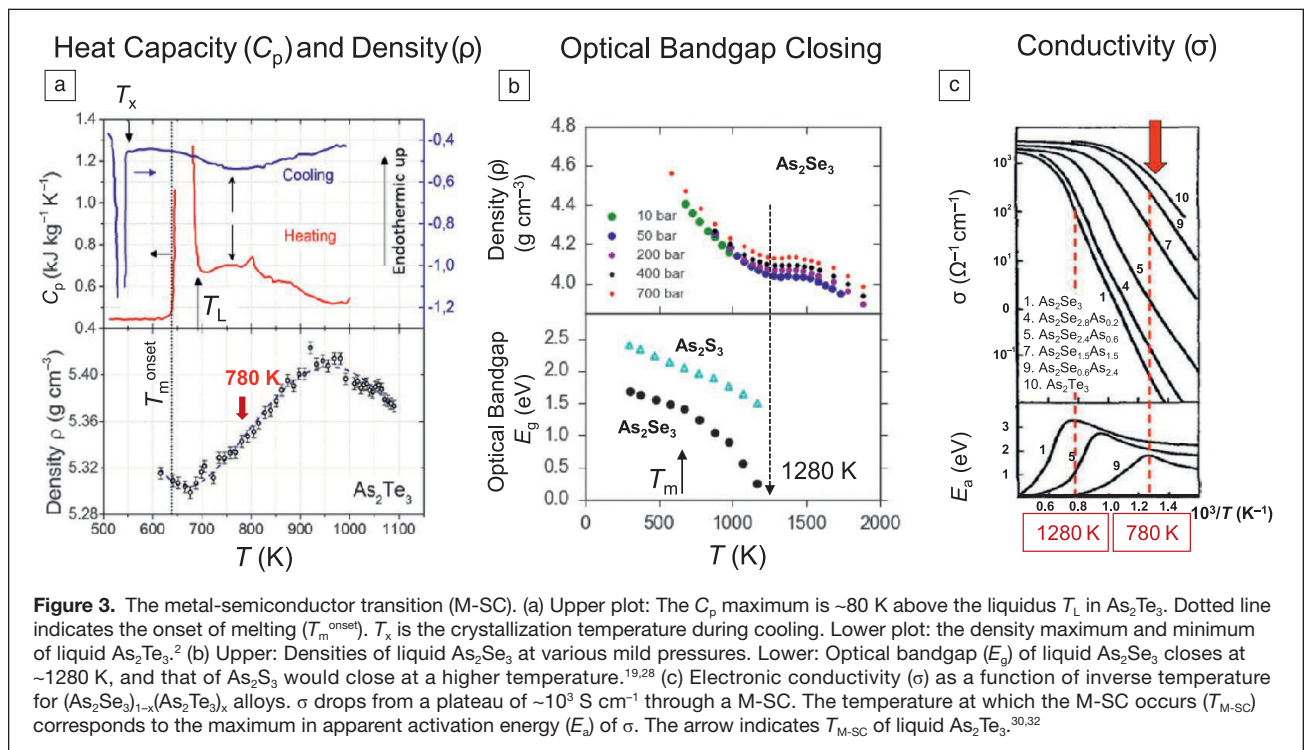
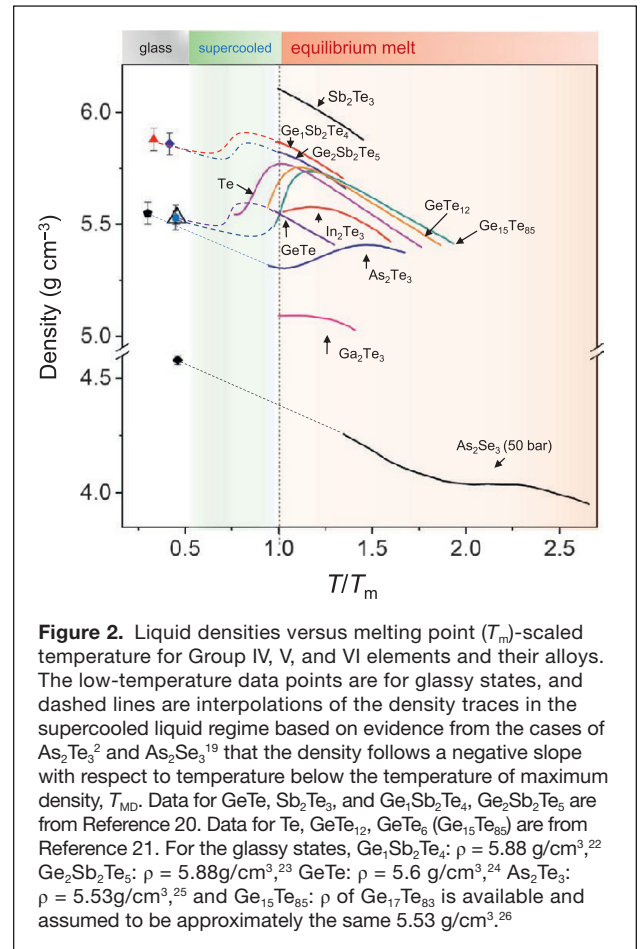


T_m -scaled temperature for the elements and several alloys. The elements and alloys exhibiting a density (ρ) maximum include Te (direct measurement), Si and Ge (by computer simulation extension of experimental data), GeTe_{12} , GeTe_6 (i.e., $\text{Ge}_{15}\text{Te}_{85}$), As_2Se_3 , As_2Te_3 , and Ga_2Te_3 as well as In_2Te_3 ²⁷ and $\text{Te}_x\text{-Se}_{1-x}$ ²⁸ (not shown). The T_{MD} is $\sim 0.9 T_m$ for tellurium. Liquid silicon undergoes a first-order liquid-liquid transition during supercooling seen as a sharp density decrease at around $0.65 T_m$ in computer simulations.²⁹ Most observable density maxima are above T_m (i.e., $T_{\text{MD}} > T_m$). Those with compositions typical of PCMs such as GeTe , Sb_2Te_3 , and $\text{Ge}_1\text{Sb}_2\text{Te}_4$, $\text{Ge}_2\text{Sb}_2\text{Te}_5$ on the Yamada line, do not display a density maximum above T_m .²⁰ But when we include the measured density of the glassy phase obtained by sputtering or hyperquenching (i.e., excessively fast cooling) and compare with the behavior of nearby compositions that do exhibit density maxima, it is highly plausible to interpolate the curves for temperature-dependence of density with maxima.

Note that between the density maximum and the density minimum, there lies an extremum in thermal expansivity, $\alpha_p = V^{-1}(\partial V/\partial T)$, where V is the volume. The temperature of the peak in α_p corresponds to the peak in the heat capacity (see next section). It also corresponds closely with temperature of the closing of the bandgap (see **Figure 3**^{19,28}), and other properties that relate to a M-SC. It is obvious that the width of the $\alpha_p(T)$ peak will be correlated with the sharpness of the maximum in $\rho(T)$.

Heat capacity anomalies

Where heat capacities have been measured for the systems shown in **Figure 2**, they show maxima that coincide with the



maximum in α_p mentioned in the previous section. The widths of these peaks are also comparable. The sharpest C_p anomalies have been observed for elemental Te and the $\text{Ge}_{15}\text{Te}_{85}$ eutectic alloy,³¹ which have been correlated with a fragile-strong transition in the viscosity that will be discussed in a later section. These sharp anomalies lie at or below the thermodynamic T_m . Cases observable above T_m tend to be broader, but are easier to study. The case of As_2Te_3 in particular has been characterized by not only C_p and density measurements, which are assembled in Figure 3, but also Knight shift² and electronic conductivity data.

Metal-semiconductor transition versus metallicity in PCMs

The maxima in thermodynamic response functions are, in each case, accompanied by conductivity transitions in Group IV, V, and VI alloys in which conductivities σ decrease from almost temperature-independent values slightly above $\sigma = 1000 \text{ S cm}^{-1}$ (Mott’s “minimum metallic conductivity”), to the lower and temperature-dependent values characteristic of semiconductors³² (Figure 3c). The transition, designated M-SC, is also evident in the closing of the optical bandgap E_g as shown for the case of As_2Se_3 liquid³³ (Figure 3b).

Considering the series As_2S_3 , As_2Se_3 , and As_2Te_3 , in Figure 3, it is clear that the M-SC transition moves to lower temperatures as the chalcogenide becomes more metallic, and the same is true for the series Sb_2S_3 , Sb_2Se_3 , and Sb_2Te_3 (the latter of which actually melts to the metallic phase, see Figure 8 of Reference 11). Finally, the trend holds for the binary solutions Se-Te.³⁴ In an attempt to quantify this trend, we introduce a new parameter, the “metallicity,” which we define as the inverse of the composition-averaged electronegativity of the alloy, according to:

$$M_p = 1 / (x_1 \cdot \chi_{p1} + x_2 \cdot \chi_{p2} + \dots + x_i \cdot \chi_{pi}),$$

where $0 < x_i < 1$ is the atomic fraction of the alloy component i , and χ_{pi} is available for each element in any Table of revised Pauling electronegativities³⁵ (hence, the subscript P).

In Figure 4a,^{36–38} we use this parameter to rationalize the variation of the temperature of the M-SCs when scaled by the alloy melting points (or liquidus for Te-Se), referred to as the reduced M-SC temperature:

$$t_{M-SC} = T_{M-SC} / T_m.$$

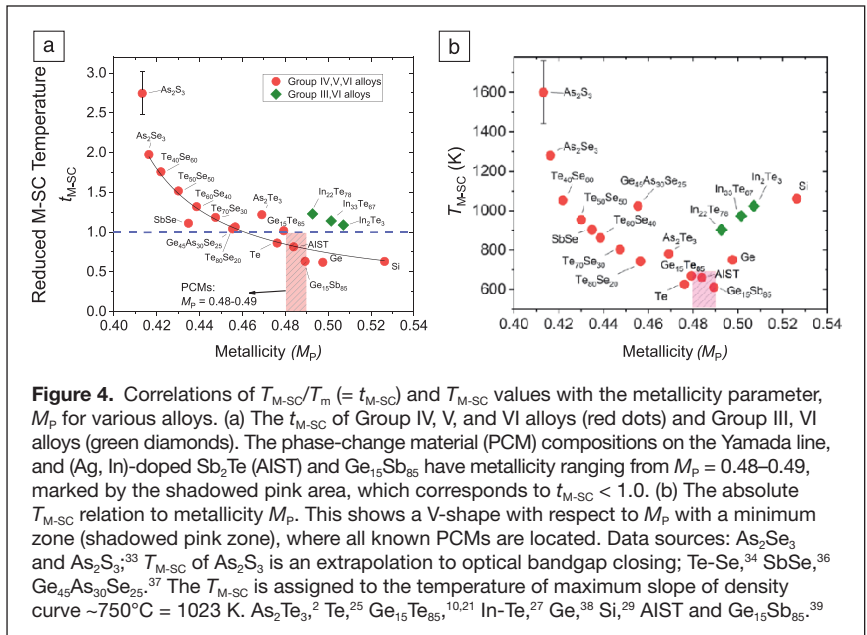
For low M_p chalcogenides such as As_2Se_3 and $\text{Te}_{40}\text{Se}_{60}$, the t_{M-SC} is larger than 1.0. With increasing metallicity, t_{M-SC} decreases, approaching the value of 1.0 around $M_p = 0.47–0.48$. For any IV, V, and VI alloy with $M_p > 0.48$, t_{M-SC} the M-SC transition falls below T_m . While the correlation is clear for Group IV, V, and VI alloys, the Group III, VI alloys (e.g., In-Te,

green diamonds) are displaced, suggesting that a volume scaling might also be a needed addition.

For PCM compositions on the Yamada line (e.g., $\text{Ge}_x\text{Sb}_{2-x}\text{Te}_4$ and $\text{Ge}_2\text{Sb}_2\text{Te}_5$), M_p lies between 0.481 and 0.487 (pink shadow area), and the Figure 4 correlation line suggests their M-SCs, should all be “submerged” below T_m ($t_{M-SC} < 1.0$), as our earlier study suggested.¹¹ Note that the PCM compositions $\text{Ge}_{15}\text{Sb}_{85}$ and (Ag, In-doped) Sb_2Te are not on the Yamada line, but they have similar values of M_p , namely in the range 0.48–0.49.³⁹

In Figure 4b, the absolute values of T_{M-SC} are plotted against M_p , showing a V-shape, where all known PCM compositions are located in the minimum zone around $M_p = 0.48–0.49$. This zone appears to be crucial for Group IV, V, and VI PCMs, as it corresponds to a lowest T_{M-SC} , and meanwhile, ensures $t_{M-SC} < 1$. Their relevance to fast switching lies on a transition in kinetic properties at the same temperature T_{M-SC} , known as a fragile-strong transition (which is discussed in detail in the next section). Only when $t_{M-SC} < 1$, the temperature window of the fragile liquid is below T_m . As such, the fragile liquid provides high atomic mobility, which facilitates crystallization that can only occur below T_m .

Following these successes, we have noted that the element bismuth (Bi) has nearly the same metallicity as Ge (0.495 and 0.498, respectively), which might be predicted to replace Ge in PCM formulations. We find that Bi_2Te_3 has been identified by atomic probe tomography as having the bonding of a PCM,⁴⁰ and Bi_2Te_3 nanowires exhibit memory switching behavior.⁴¹ It raises the question, “is there perhaps an equivalent of the “Yamada line” in the Bi-Sb-Te system (Ge-free) (e.g., along much of the Bi_2Te_3 - Sb_2Te_3 join)?” Both are in the weak metal state at their melting temperatures, as for PCMs. Attention has already been drawn to the analog of the GST Yamada line provided by the (Ge-containing) Ge-Bi-Te system⁴² and to the similarity of the various crystalline structures along that line



to those in the GST system. In that case, it was reported that the presence of Bi “significantly enhances the crystallization of the GBT layers.”

Finally, we caution that the use of the metallicity parameter should be limited to the covalent alloys based on the Group IV, V, and VI elements. These elements are metalloid or close to metalloid, where the inverse electronegativity gives a quantitative measure of how “metallic” the element is. Those alloys with a higher metallicity are usually associated with higher conductivities. This may explain why, for liquid PCMs (with high metallicities), the conductivity upon heating usually reaches the value of 10^2 – 10^3 S cm⁻¹ of a “weak-metal” state earlier at a relatively low temperature (often below T_m), at which the semiconductor-to-metal transition occurs. By contrast, non-PCM chalcogenides need to be heated to higher temperatures, usually above T_m , so as to reach the weak-metal state for the semiconductor-to-metal transition to occur.

Note that there are density functional theory (DFT)-based parameter maps proposed for crystalline phase properties of PCMs.^{43,65} However, they are not available for amorphous phases. It remains to be seen whether and how they are related to the metallicity parameter introduced here and the M-SC behaviors.

Double-kink and smeared-out fragile-strong transitions in viscosity

In their classic 1965 paper,⁴⁴ Adam and Gibbs presented a molecular kinetic theory in which the temperature dependence of relaxation time $\tau(T)$ is determined by the probability of cooperative rearrangement of mobile units in the system. The latter can be expressed in terms of configurational entropy, S_c :

$$\tau = \tau_0 \exp[-C/(TS_c)]$$

where τ_0 is the pre-exponent near the phonon cycle time (10^{-14} s) and C is a constant. In treating experimental data, S_c has been shown to be proportional to the excess entropy S_{ex} of liquid over crystal, which can be derived from C_p .¹⁰ Thus, the C_p maximum leads to a transition in $\tau(T)$ and therefore the viscosity $\eta(T)$ (through the Maxwell relation $\eta = G_\infty \tau$, where G_∞ is the infinite-frequency shear modulus.)

The drastic change in the temperature dependence of viscosity from a high-temperature fragile liquid to a low-temperature strong liquid near T_g is the so-called fragile-strong transition (FST). According to the liquid fragility concept,⁴⁵ some liquids, exhibiting a near-Arrhenius rise in

viscosity on approaching T_g , are classified as “strong” liquids, while others, showing a range of non-Arrhenius behavior, are referred to “fragile” liquids. Fragility is commonly characterized by measuring the slope of the T_g -scaled Arrhenius plot (fragility plot) at T_g , called “steepness index” or “ m -fragility,” $m = d \log \eta / d(T_g/T) |_{T=T_g}$.⁴⁵

A clear FST is demonstrated in Ge₁₅Te₈₅ (Figure 5)^{8,10–12,45,47,48,53,57–64} as a “double-kink” in $\eta(T)$ -curve near its eutectic temperature, which is verified by a direct differential scanning calorimetry (DSC) measurement near T_g .¹⁰ The corresponding structural change is shown as a stepwise rise in the second to first peak position ratio r_2/r_1 of reduced pair distribution functions $G(r)$ from *in situ* x-ray scattering.⁴⁶ In As₂Te₃, the FST is so smeared-out that no “double-kink” is discerned. The C_p anomaly spans ~300 K (Figure 3a). The viscosity of As₂Te₃ drops smoothly by ~3 orders of magnitude in

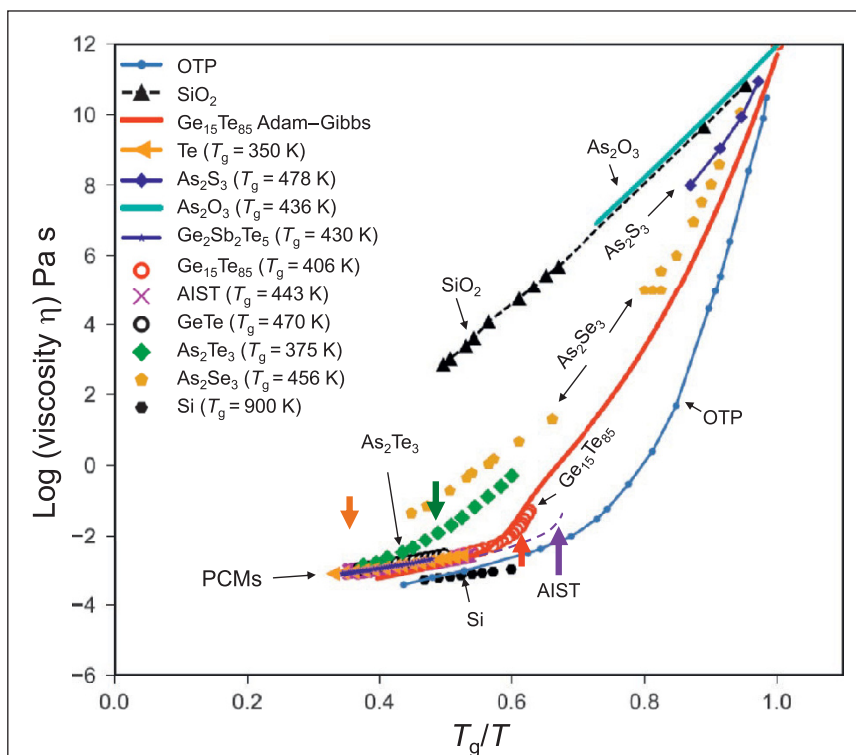


Figure 5. Arrhenius plots scaled by the glass-transition temperature (T_g) for the viscosity (η) of Group IV, V, and VI alloys. Phase-change materials (PCMs), which have the highest metallicity, exhibit the lowest viscosities at T_m (where $T_g/T_m \sim 0.5$). On the T_g -reduced scale, they overlap the elemental Te data. Alloys of lower metallicity exhibit systematically higher viscosities, and lower m fragilities. The lowest metallicity case, As₂O₃, with $m = 19$ (according to light-scattering relaxation time data) is even stronger than the archetypal strong liquid, SiO₂. Apart from this interesting case, Figure 5 contains only directly measured experimental viscosities. The crystal-growth-derived viscosities are not shown. The bold colored arrows indicate T_{m-SC} (660 K) of AIST (purple) below T_m , and that of As₂Te₃ (green), Ge₁₅Te₈₅ (red), and As₂Se₃ (orange) above T_m , respectively. Data sources: Ge₂Sb₂Te₅,⁵⁷ $T_g = 430$ K,⁵⁸ although the value is still under debate;⁸ AIST (Ag-In-doped Sb₂Te),⁴⁷ (its $T_g = 443$ K⁵⁹) is also under debate;⁴⁸ Te;⁵⁹ $T_g = 350$ K;¹¹ Ge₁₅Te₈₅: viscosity data,⁶⁰ Adam-Gibbs fitting line;¹⁰ GeTe⁵³ assigned $T_g = 470$ K; As₂Te₃,⁶¹ $T_g = 375$ K is the value at which calculated viscosity reaches 10^{12} Pa s; As₂Se₃,⁶² As₂S₃.⁴⁵ For As₂O₃, relaxation times were directly measured using light scattering, from which the precise Vogel-Fulcher-Tammann (VFT) parameters were obtained. The viscosity is represented by a VFT fit in the similar temperature range of relaxation time data using the parameters in Reference 63; SiO₂, and o-terphenyl (OTP);⁴⁵ Si⁶⁴ (the T_g of Si is unknown and here assigned as 900 K).¹⁰

the transition range. The sharpness of the FST depends on the sharpness of the C_p maximum and the associated loss of S_{ex} across the transition.

The viscosity of PCM compositions has been measured directly for (e.g., $\text{Ge}_2\text{Sb}_2\text{Te}_5$, [Ag, In]-doped Sb_2Te [AIST], and GeTe) at high temperatures above their T_m , as shown in Figure 5. Those data nearly overlap the high-temperature viscosity of Te (orange triangles) and that of the fragile state of $\text{Ge}_{15}\text{Te}_{85}$ above its FST (open circles) at $T_g/T < 0.5$. Thus, liquid PCMs above T_m exhibit a “fragile” behavior, as expected from their weak-metal states in the equilibrium melt.

Insofar as the predicted FSTs (also M-SC transitions) always occur below T_m in PCMs, they cannot be directly observed due to the interference of fast crystallization, but have only been inferred. Orava et al.^{47,48} measured the temperature-dependence of crystallization kinetics using ultrafast DSC, and inferred an “Arrhenius”-like behavior of viscosity between 383 K and ~490 K for as-deposited AIST. They proposed a broad crossover from a high-temperature fragile liquid ($m = 74$) to a low-temperature strong liquid ($m = 37$). Zalden et al.⁴⁹ identified a crossover temperature in AIST (~570 K for melt-quenched samples and ~540 K for as-deposited samples) through the kinetics of subnanosecond laser induced crystallization. In the same composition, Salinga et al.⁵⁰ revealed a nearly constant activation energy for the temperature-dependence of crystal-growth-derived viscosity below ~570 K, which they referred to as Arrhenius-like behavior. This was attributed to the falling out of equilibrium into glassy states due to extremely fast cooling rates (~ 10^9 – 10^{10} K/s) by laser-melt-quench on the small beam spot.

An *ab initio* calculation by Zhang et al. for AIST⁵¹ successfully produced reasonable temperature-dependence of diffusivity at high temperature above T_m , though it did not give a reasonable account for the supercooled liquid state at much lower temperatures. For $\text{Ge}_2\text{Sb}_2\text{Te}_5$, the ultrafast DSC study of Orava et al.⁸ implied a single fragility parameter ($m \approx 90$) for the entire liquid regime, while the *ab initio* simulation of Flores-Ruiz and Micoulaut⁵² proposed a FST from $m \geq 129$ to $m = 90$ at 792 K. An ultrafast DSC study of $\text{Ge}_2\text{Sb}_2\text{Te}_5$ nanoparticles suggested a broad FST.⁵³ In another PCM GeTe , a single fragility ($m = 76$) is suggested, partially based on ultrafast DSC measurements, to describe the liquid without a FST,⁵⁴ which is in contrast to the extrapolation from reference 11 and this work.

Zhang et al.¹⁶ emphasized a “kinetic crossover,” defined as a large change in activation energy of viscosity, that occurs somewhat below T_m , as essential for fast crystal growth in PCMs. Note that a so-defined “kinetic crossover” is not the same concept as the FST discussed here (or fragile-strong crossover), because the former is expected during the undercooling of any fragile liquid that is described by mode coupling theory (MCT)⁵⁵ at higher temperatures. It corresponds to the much-discussed crossover from MCT to “hopping” behavior (i.e., it does not imply a structural or heat capacity-based transition to a stronger liquid state).

Unlike the cases of good glass-formers (e.g., $\text{Ge}_{15}\text{Te}_{85}$ and As_2Te_3), the ambiguity and controversy of fragilities and FSTs in PCM compositions are no surprise because direct experiments cannot easily be carried out in the fast crystallization regime to determine the viscosity of supercooled liquid. In the literature, the reported crystal growth velocities themselves may differ by a few orders of magnitude, depending on different sample preparation processes and experimental approaches. Furthermore, since crystallization processes may occur in either glass or liquid, and since the glass-transition temperatures of PCMs are still debated, it is unclear whether the derived viscosity corresponds to the equilibrium viscosity, which is the meaningful quantity for discussion of liquid fragility, or something else. For instance, if a liquid falls out of equilibrium during cooling and forms a glass at a fictive temperature T_f , which depends on the cooling rate, a quantity with dimensions of viscosity can still be measured, and it usually follows the Arrhenius Law,⁵⁶ but this behavior should not be confused with that of a strong liquid, nor the transition to the strong state, a FST.

Zalden et al.³⁹ recently conducted a femtosecond pump-probe x-ray laser experiment that enables resolution of structural changes within nanosecond time scales, which provided the first direct evidence of a structural transition in PCMs below T_m . This was observed at 660 K in AIST ($\text{Ag}_4\text{In}_3\text{Sb}_{67}\text{Te}_{26}$) and 610 K in $\text{Ge}_{15}\text{Sb}_{85}$, and is so far the most convincing evidence of liquid-liquid transitions (which are also M-SCs, as mentioned earlier) in the supercooled liquid PCMs. When the results are plotted in Figure 4, the data well support our prediction from the metallicity parameter.

We further comment on the significance of FSTs due to the sharp heat capacity anomalies in the PCM metallicity domain. The FST controls the kinetic factor (atomic mobility) of nucleation and growth of crystals. In the fragile state, a high kinetic factor facilitates crystallization (fast switching) at an elevated temperature between T_{M-SC} and T_m by a “set” pulse, while, in the strong state below T_{M-SC} , a low kinetic factor hinders crystallization at ambient temperature, which is favorable for data retention. Within limits, this transition should be tunable by change of metallicity. From the previously discussed analysis, this transition is also the origin of the additional entropy loss during vitrification of PCMs, as mentioned in the Introduction section.

A recent study suggested that imminence of a M-SC/FST transition is signaled well above T_m by the combination of viscosity with diffusivity data, known as the Stokes–Einstein relation (SER).¹² In PCMs, unlike other liquids, the SER breaks down while in a high-fluidity state ($\tau \sim \text{ps}$) and even above T_m .¹²

Summary and outlook

The liquid states of PCMs are shown to be anomalous in comparison with the majority of liquid (and glass-forming) chalcogenides. This appears to be due to the existence of M-SC transitions, hidden below T_m , which are driven by structure-related thermodynamic and kinetic anomalies. The knowledge of the transition-related property changes is essential

for understanding of switching behaviors. The M-SC for a wide range of compositions seems to be confined to a narrow range of values of a new parameter, the metallicity M_p . Given that all PCMs are concentrated in a zone of $M_p = 0.48\text{--}0.49$, the metallicity concept may provide useful guidance for future PCM designs.

Acknowledgments

P.L. acknowledges financial support from the National Science Foundation (NSF)–Division of Materials Research under Grant No. 1832817. C.A.A. acknowledges financial support from NSF Chemistry Division under Grant Nos. CHE-1213265 and CHE-185606. S.W. is grateful for discussion with P. Zalden and comments of M. Wuttig.

References

1. B.J. Eggleton, B. Luther-Davies, K. Richardson, *Nat. Photonics* **5**, 141 (2011).
2. Y.S. Tverjanovich, V.M. Ushakov, A. Tverjanovich, *J. Non Cryst. Solids* **197**, 235 (1996).
3. S.R. Ovshinsky, *Phys. Rev. Lett.* **21**, 1450 (1968).
4. N. Yamada, E. Ohno, N. Akahira, K. Nishiuchi, K. Nagata, M. Takao, *Jpn. J. Appl. Phys.* **26**, 61 (1987).
5. N. Yamada, E. Ohno, K. Nishiuchi, N. Akahira, M. Takao, *J. Appl. Phys.* **69**, 2849 (1991).
6. M. Wuttig, *Nat. Mater.* **4**, 265 (2005).
7. M. Wuttig, N. Yamada, *Nat. Mater.* **6**, 824 (2007).
8. J. Orava, L. Greer, B. Gholipour, D.W. Hewak, C.E. Smith, *Nat. Mater.* **11**, 279 (2012).
9. D. Loke, J.M. Skelton, W.-J. Wang, T.-H. Lee, R. Zhao, T.-C. Chong, S.R. Elliott, *Proc. Natl. Acad. Sci. U.S.A.* **111**, 13272 (2014).
10. S. Wei, P. Lucas, C.A. Angell, *J. Appl. Phys.* **118**, 034903 (2015).
11. S. Wei, G.J. Coleman, P. Lucas, C.A. Angell, *Phys. Rev. Appl.* **7**, 034035 (2017).
12. S. Wei, Z. Evenson, M. Stolpe, P. Lucas, C.A. Angell, *Sci. Adv.* **4**, eaat8632 (2018).
13. S. Bordas, M.T. Clavaguer-Mora, B. Legendre, C. Hancheng, *Thermochim. Acta* **107**, 239 (1986).
14. H.S.P. Wong, S. Raoux, S. Kim, J. Liang, J.P. Reifenberg, B. Rajendran, M. Asheghi, K.E. Goodson, *Proc. IEEE* **98**, 2201 (2010).
15. M. Wuttig, V.L. Deringer, X. Gonze, C. Bichara, J.-Y. Raty, *Adv. Mater.* **30**, 1803777 (2018).
16. W. Zhang, R. Mazzarello, M. Wuttig, E. Ma, *Nat. Rev. Mater.* **4**, 150 (2019).
17. C.A. Angell, *Ann. Rev. Phys. Chem.* **34**, 593 (1983).
18. C.A. Angell, U. Essman, M. Hemmati, P.H. Poole, F. Sciortino, *Physica A* **205**, 122 (1994).
19. S. Hosokawa, Y. Sakaguchi, K. Tamura, *J. Non Cryst. Solids* **150**, 35 (1992).
20. C. Otjacques, J.-Y. Raty, J.-P. Gaspard, Y. Tsuchiya, C. Bichara, in *Collection SFN* (EDP Sciences, 2011), pp. 233–245.
21. Y. Tsuchiya, *J. Phys. Condens. Matter* **3**, 3163 (1991).
22. C. Steimer, V. Coulet, W. Welnic, H. Dieker, R. Detemple, C. Bichara, B. Beuneu, J.-P. Gaspard, M. Wuttig, *Adv. Mater.* **20**, 4535 (2008).
23. W.K. Njoroge, H.-W. Wöltgens, M. Wuttig, *J. Vac. Sci. Technol. A* **20**, 230 (2002).
24. K.L. Chopra, S.K. Bahl, *J. Appl. Phys.* **40**, 4171 (1969).
25. R.K. Quinn, *Mater. Res. Bull.* **9**, 803 (1974).
26. F. Betts, A. Bienenstock, D.T. Keating, J.P. deNeufville, *J. Non Cryst. Solids* **7**, 417 (1972).
27. H. Thurn, J. Ruska, *Z. Anorg. Allg. Chem.* **426**, 237 (1976).
28. S. Hosokawa, S. Yamada, K. Tamura, *J. Non Cryst. Solids* **156**, 708 (1993).
29. S. Sastry, C.A. Angell, *Nat. Mater.* **2**, 739 (2003).
30. P. Nagels, M. Rotti, S. Vikhrov, *J. Phys. Colloq.* **42**, C4 (1981).
31. Y. Tsuchiya, *J. Non Cryst. Solids* **312–314**, 212 (2002).
32. V.A. Alekseev, A.A. Andreev, M.V. Sadovskii, *Sov. Phys. Usp.* **23**, 551 (1980).
33. S. Hosokawa, Y. Sakaguchi, H. Hiasa, K. Tamura, *J. Phys. Condens. Matter* **3**, 6673 (1991).
34. F. Kakinuma, S. Ohno, *J. Phys. Soc. Jpn.* **56**, 619 (1987).
35. A.L. Allred, *J. Inorg. Nucl. Chem.* **17**, 215 (1961).
36. F. Kakinuma, S. Ohno, K. Suzuki, *J. Non Cryst. Solids* **117**, 575 (1990).
37. H. Krebs, J. Ruska, *J. Non Cryst. Solids* **16**, 329 (1974).
38. M.H. Bhat, V. Molinero, E. Soignard, V.C. Solomon, S. Sastry, J.L. Yarger, C.A. Angell, *Nature* **448**, 787 (2007).
39. P. Zalden, F. Quirin, M. Schumacher, J. Siegel, S. Wei, A. Koc, M. Nicoul, M. Trigo, P. Andreasson, H. Enquist, M.J. Shu, T. Pardini, M. Chollet, D. Zhu, H. Lemke, I. Ronneberger, J. Larsson, A.M. Lindenberg, H.E. Fischer, S. Hau-Riege,

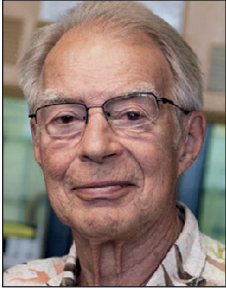
- D.A. Reis, R. Mazzarello, M. Wuttig, K. Sokolowski-Tinten, *Science* **364**, 1062 (2019).
40. M. Zhu, O. Cojocar-Mirédin, A.M. Mio, J. Keutgen, M. Küpers, Y. Yu, J.-Y. Cho, R. Dronskowski, M. Wuttig, *Adv. Mater.* **30**, 1706735 (2018).
41. N. Han, S.I. Kim, J.-D. Yang, K. Lee, H. Sohn, H.-M. So, C.W. Ahn, K.-H. Yoo, *Adv. Mater.* **23**, 1871 (2011).
42. T.-Y. Lee, C. Kim, Y. Kang, D.-S. Suh, K.H.P. Kim, Y. Khang, *Appl. Phys. Lett.* **92**, 101908 (2008).
43. J.-Y. Raty, M. Schumacher, P. Golub, V.L. Deringer, C. Gatti, M. Wuttig, *Adv. Mater.* **31**, 1806280 (2019).
44. G. Adam, J.H. Gibbs, *J. Chem. Phys.* **43**, 139 (1965).
45. C.A. Angell, *Science* **267**, 1924 (1995).
46. S. Wei, M. Stolpe, O. Gross, W. Hembree, S. Hechler, J. Bednarcik, R. Busch, P. Lucas, *Acta Mater.* **129**, 259 (2017).
47. J. Orava, H. Weber, I. Kaban, A.L. Greer, *J. Chem. Phys.* **144**, 194503 (2016).
48. J. Orava, D.W. Hewak, A.L. Greer, *Adv. Funct. Mater.* **25**, 4851 (2015).
49. P. Zalden, A. von Hoegen, P. Landreman, M. Wuttig, A.M. Lindenberg, *Chem. Mater.* **27**, 5641 (2015).
50. M. Salinga, E. Carria, A. Kaldenbach, M. Bornhöff, J. Benke, J. Mayer, M. Wuttig, *Nat. Commun.* **4**, 2371 (2013).
51. W. Zhang, I. Ronneberger, P. Zalden, M. Xu, M. Salinga, M. Wuttig, R. Mazzarello, *Sci. Rep.* **4**, 6529 (2014).
52. H. Flores-Ruiz, M. Micoulaut, *J. Chem. Phys.* **148**, 034502 (2018).
53. H. Weber, J. Orava, I. Kaban, J. Pries, A.L. Greer, *Phys. Rev. Mater.* **2**, 093405 (2018).
54. B. Chen, G.H. ten Brink, G. Palasantzas, B.J. Kooi, *J. Phys. Chem. C* **121**, 8569 (2017).
55. W. Götz, *J. Phys. Condens. Matter* **11**, A1 (1999).
56. C.A. Angell, K.L. Ngai, G.B. McKenna, P.F. McMillan, S.W. Martin, *J. Appl. Phys.* **88**, 3113 (2000).
57. M. Schumacher, H. Weber, P. Jónvári, Y. Tsuchiya, T.G. Youngs, I. Kaban, R. Mazzarello, *Sci. Rep.* **6**, 27434 (2016).
58. J.A. Kalb, M. Wuttig, F. Spaepen, *J. Mater. Res.* **22**, 748 (2007).
59. F. Herwig, M. Wobst, *Z. Für Met.* **83**, 35 (1992).
60. H. Neumann, F. Herwig, W. Hoyer, *J. Non Cryst. Solids* **205–207** (Pt. 1), 438 (1996).
61. A. Tverjanovich, *J. Non Cryst. Solids* **298**, 226 (2002).
62. A.S. Tverjanovich, *Glass Phys. Chem.* **29**, 532 (2003).
63. S.N. Yannopoulos, G.N. Papatheodorou, G. Fytas, *Phys. Rev. B* **60**, 15131 (1999).
64. W.-K. Rhim, K. Ohsaka, *J. Cryst. Growth* **208**, 313 (2000).
65. J. Pries, O. Cojocar-Mirédin, M. Wuttig, *MRS Bull.* **44** (9), 699 (2019). □



Shuai Wei is a postdoctoral researcher at RWTH Aachen University, Germany. He received his PhD degree in materials science in 2014 from Saarland University, Germany. He was a Humboldt Feodor-Lynen Fellow at Arizona State University and The University of Arizona. His research focuses on thermodynamics, kinetics, and structures of amorphous phase-change materials and bulk metallic glasses (amorphous metals). His awards include the RWTH Start-Up Fund, the Humboldt Feodor Lynen Fellowship, the Dr.-Eduard-Martin Award, a Materials Research Society Graduate Student Silver Award, and the Kühborth Award. Wei can be reached by email at swei@physik.rwth-aachen.de.

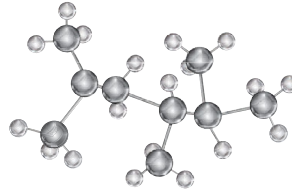


Pierre Lucas is a professor of materials science and engineering, and a professor of optical science at The University of Arizona. He received his PhD degree in physical chemistry from Arizona State University in 1999. He has authored more than 100 peer-reviewed articles and book chapters in the field of materials, calorimetry, and optics. He was past chair of the Glass and Optical Materials Division of The American Ceramic Society and is a senior member of SPIE, The International Society for Optics and Photonics. Lucas can be reached by email at Pierre@u.arizona.edu.



Austen Angell is a Regents' Professor at Arizona State University (ASU). He received his BSc and MSc degrees from the University of Melbourne, Australia, and his PhD degree from Imperial College London, UK. He completed postdoctoral research at Argonne National Laboratory, and then joined Purdue University in 1966, moving to ASU in 1989. His research interests focus on supercooled liquids and glasses, particularly water and ionic liquids, anomalous liquids, and batteries. He has authored approximately 540 papers and reviews, with an H-index of 110 (Google scholar). His awards include the George W. Morey Award from The American

Ceramic Society, the Joel Henry Hildebrand Award from the American Chemical Society, the David Turnbull Lectureship Award from the Materials Research Society, and the Max Bredig Award from The Electrochemical Society. Angell can be reached by email at caa@asu.edu.



23rd International Conference on Ion Implantation Technology

September 20–24, 2020 | San Diego, California | The US Grant Hotel

SAVE THE DATE

The **International Conference on Ion Implantation Technology 2020 (IIT 2020)** is the 23rd Conference in the biannual series focused on discussion of major challenges in current and emerging technologies related to implant/doping and annealing processes, device applications, equipment, metrology and modeling. The Conference offers an excellent opportunity for engineers and researchers in industry, research institutes and universities to present new results and to discuss ideas of new applications of ion implantation and annealing. The organizers welcome contributions from a wide range of topics, from fundamental research to industrial applications and equipment.

SCIENTIFIC PROGRAM

The five-day Conference will feature the following topics:

- Advanced Implant/Doping and Annealing Equipment
- Annealing Technologies and Processes
- Device Applications for Implant/Doping and Annealing Processes
- Implant/Doping Technologies and Processes
- Metrologies for Implant/Doping and Annealing Processes
- Modeling and Simulation of Implant/Doping and Annealing Processes

GENERAL CHAIR

Mitch Taylor, Mitch Taylor Consulting

TECHNICAL PROGRAM CHAIR

Susan Felch, Susan Felch Consulting

SPONSORSHIPS CHAIR

Aaron Vanderpool, Intel Corporation

ANNEALING PROGRAM CHAIR

Wilfried Lerch, SkyLark Solutions

PROCEEDINGS CHAIR

Larry Larson, Texas State University at San Marcos

For additional information, visit MRS.ORG/IIT2020.

IIT 2020 is managed by

